American Mineralogist, Volume 80, pages 144–161, 1995

Significance of pyroxene megacrysts for massif anorthosite petrogenesis: Constraints from the Labrieville, Quebec, pluton

Brent E. Owens, Robert F. Dymek
Department of Earth and Planetary Sciences, Washington University, Saint Louis, Missouri 63130, U.S.A.

Abstract

Newly discovered orthopyroxene and clinopyroxene megacrysts (OPMs and CPMs) in the Labrieville massif provide additional constraints on megacryst origins and their significance in massif anorthosite petrogenesis. Pyroxene megacrysts (~1–15 cm across) occur throughout the anorthosite, some in layered zones (as cumulates?) and others as scattered crystals that form subophitic intergrowths with plagioclase; some also contain tabular plagioclase inclusions. In many cases, pyroxene megacrysts are intergrown with ilmenite and locally occur within meter-sized masses of ilmenite. Plagioclase and ilmenite are the dominant exsolution products in OPMs, whereas CPMs contain additional lamellae of orthopyroxene. Biotite consistently occurs with megacrysts, locally as an integral portion of exsolution lamellae.

Microprobe spot compositions of the megacrystic pyroxenes (OPM ~ En_{58-66}, CPM ~ $Wo_{45}En_{40}Fs_{15}$) are essentially the same as those of smaller matrix pyroxenes in the same outcrops. In contrast, three bulk OPMs (4.4–5.9 wt% Al_2O_3) and one CPM (6.4 wt% Al_2O_3) are enriched in Ca, Na, Al, and Ti, compatible with observed exsolution products. Plagioclase lamellae (An_{34-53}) are more calcic than matrix plagioclase (An_{32-38}) but are the most sodic recognized in any massif anorthosite thus far.

Field characteristics of megacrysts indicate that they formed contemporaneously with the other minerals in the same outcrops. Furthermore, bulk OPMs have X_{Mg} similar to matrix pyroxene (or are slightly more Fe-rich). In comparison, OPMs from the Saint Urbain massif are more magnesian (~En_{66-72}), whereas lamellae and matrix plagioclase are more anorthitic (~An_{55-75} and ~An_{40}, respectively). These systematic differences between the two massifs suggest that the En content of OPMs and the An content of plagioclase (matrix and lamellae) are strongly controlled by local magma composition. Collectively, these results can be explained best by the in-situ growth of megacrysts, together with or after adjacent plagioclase. The megacrysts bulk compositions can be adequately accounted for by a rapid growth mechanism. The common association of OPMs with ilmenite (and biotite) is noteworthy and suggests that oxidizing conditions played an important role in controlling the properties and compositions of the megacrysts. The implication is that these megacrysts are not relics of prior high-pressure pyroxene fractionation and provide no demonstrable link to a basaltic parent magma for this massif.

Introduction

Pyroxene megacrysts containing composite lamellae of plagioclase and iron titanium oxide have played a prominent role in recent models for the origin and crystallization history of massif anorthosites. Currently, most investigators would agree that the lamellae are of exsolution origin and that the primary compositions of the megacrysts were Al-rich. However, there is substantial disagreement regarding the nucleation site of the megacrysts, the mechanism of Al enrichment, and the corresponding implications of such crystals for the evolution of massif anorthosite complexes. As a further contribution towards unraveling the petrogenetic significance of such megacrysts, we report in this paper new results on recently discovered examples from the Labrieville anorthosite massif, Quebec. We use these results, in conjunction with additional observations from the Saint Urbain anorthosite massif, Quebec, as a basis for a more general evaluation of the megacryst problem.

A partisan review of the megacryst problem

The first extended description and illustration of orthopyroxene megacrysts (OPMs) appears to be that of Hargraves (1962, p. 166), who reported "anorthosite with coarse pyroxene crystals" in the Allard Lake massif, Quebec. Hargarves did not, at the time, recognize the aluminous nature of such crystals, nor the presence of plagioclase lamellae. However, he did observe that some megacrysts poikilitically enclose plagioclase and that many occur in layered zones, although others seem to form pla-

0003–004X/95/0102–0144$02.00

nar arrays that transgress primary layering. He also called attention to similar reports, dating back to Michot (1939), of large pyroxenes from other massif anorthosites and noted that many investigators called upon the action of volatiles to account for the large size of the OPMs.

Savolahti (1966) described large hypersthene crystals in pegmatitic anorthosite from the Ahvenisto massif, Finland, and reported an analysis of the core of one such grain that showed 7.45 wt% Al_2O_3. These cores contain lamellae that Savolahti was unable to identify in thin section, but plagioclase inclusions were discovered during mineral separation. We suspect that the lamellae are plagioclase.

Philpotts (1966) observed OPMs as well as clinopyroxene megacrysts (CPMs) in anorthositic rocks from Grenville Township, Quebec, and noted the presence of plagioclase lamellae in some crystals. Philpotts showed that OPMs and CPMs both are aluminous (~3.9 and 5.3 wt% Al_2O_3, respectively, in the two crystals he analyzed), which he interpreted to reflect formation in an Al-rich environment. Although Philpotts concluded that the plagioclase lamellae represented magmatic pyroxene + plagioclase intergrowths, he considered the idea of an exsolution origin to have merit.

Emslie (1975) framed the problem of pyroxene megacrysts in its modern context. He recognized that megacrysts occur in many massif anorthosites and must therefore represent an integral part of the process of anorthosite formation. He presented analyses from several localities showing that the OPMs contain high amounts of Al_2O_3 (~3–9 wt%), which he interpreted as indicating crystallization at high pressure. Emslie argued that the OPMs precipitated from basaltic magma at great depth and were subsequently transported to shallower crustal levels as xenocrysts in their host anorthosite. Emslie further reasoned that decompression resulted in the exsolution of plagioclase lamellae, which formed from $NaAlSi_2O_6$ (jadeite) and $CaAl_2SiO_6$ (Tschermak) components in the original orthopyroxene.

At about the same time, Morse (1975) noted that OPMs occur at several levels within a layered sequence of the Nain anorthsite complex, Labrador, and that many crystals form subophitic intergrowths with plagioclase. Morse interpreted the OPMs as products of in-situ crystallization, and he attributed their aluminous compositions to rapid growth in an Al-rich environment, with plagioclase exsolving upon cooling. In addition, Morse recognized that plagioclase exsolution from pyroxene requires a source of silica. The presence of additional exsolved platelets of iron titanium oxide (magnetite) in the OPMs led Morse to postulate the following two-stage reaction: (1) $3FeSiO_3 + \frac{1}{2}O_2 \rightarrow Fe_3O_4 + 3SiO_2$; (2a) $CaAl_2SiO_6 + SiO_2 \rightarrow CaAl_2Si_2O_8$ and (2b) $NaAlSi_2O_6 + SiO_2 \rightarrow NaAlSi_3O_8$. Thus, oxidation of the $FeSiO_3$-component in orthopyroxene liberates the silica required for plagioclase exsolution.

Dymek and Gromet (1984) reported on OPMs from the Saint Urbain massif, Quebec, and noted that (1) OPMs form subophitic intergrowths with matrix plagioclase and are commonly intergrown with biotite along their margins; (2) OPMs locally contain tabular plagioclase inclusions with compositions similar to surrounding matrix plagioclase; (3) OPMs have nearly the same En content as other orthopyroxenes throughout the massif, including matrix pyroxenes in the same samples ($\sim En_{70-75}$), but are enriched in Ca, Al, Ti, Fe^{3+}, and REE; (4) OPMs are aluminous (~4–6 wt%), but characterized by a preponderance of $^{[4]}Al$ over $^{[6]}Al$, needed to charge balance $^{[6]}Ti$ and $^{[6]}Fe^{3+}$; (5) exsolution lamellae in OPMs are composites of ilmenite (an exsolution intergrowth of hematite and ilmenite in this case) and plagioclase having An contents greater than matrix plagioclase ($\sim An_{50-75}$ vs. $\sim An_{40}$).

Dymek and Gromet (1984) interpreted the field relationships and petrography as indicating that the OPMs nucleated and grew in situ after plagioclase, rather than at some remote (deep) site. As such, OPMs are not primitive crystals, a conclusion supported by their similar values of X_{Mg} and higher concentrations of REE (up to an order of magnitude) compared with matrix orthopyroxene. Thus, the OPMs provide no link to a parental basaltic magma for this massif. Dymek and Gromet further postulated that the OPMs achieved their aluminous and REE-rich compositions as a result of metastable growth at high temperature in feldspathic liquids. They attributed exsolution of the ilmenite and plagioclase lamellae to decomposition of minor element components ($CaAl_2SiO_6$, $CaFe^{2+}_{0.5}Ti_{0.5}AlSiO_6$, $CaFe^{3+}AlSiO_6$) during slow cooling from magmatic conditions, with the silica needed to form plagioclase provided by simultaneous decomposition of an Eskola component ($\square Ca_{0.5}AlSi_2O_6$), without oxidation.

Maquil and Duchesne (1984) and Duchesne et al. (1985) reported on OPMs from the Rogaland Complex, Norway, and observed that megacrysts are enriched in Cr and Al compared with other orthopyroxenes. They interpreted these features as evidence for polybaric crystallization during ascent of the anorthosite plutons, with OPMs crystallizing at high pressure and other orthopyroxenes at low pressure.

Jaffe and Schumacher (1985) reported garnet within exsolution lamellae in OPMs from the Adirondack (Marcy) massif. They regarded the garnet as evidence for an exotic, high-pressure origin for the megacrysts, which were subsequently emplaced into fractures in gabbroic anorthosite at shallower levels. Jaffe and Schumacher (1985) endorsed the suggestion of Dymek and Gromet (1984) that decomposition of an Eskola component played a central role in the exsolution of plagioclase. Previously, Bohlen and Essene (1978) had described OPMs in the Marcy anorthosite and suggested that high-temperature crystallization from plagioclase-rich melts was sufficient to account for their aluminous compositions without resorting to formation at high pressure.

In summary, there are two fundamental questions posed by pyroxene megacrysts and two contrasting answers: their site of formation (local vs. remote); and the mechanism (metastable vs. high-pressure growth) whereby they achieved their distinctive bulk compositions. The interpretation of OPMs as relics of high-pressure crystalliza-

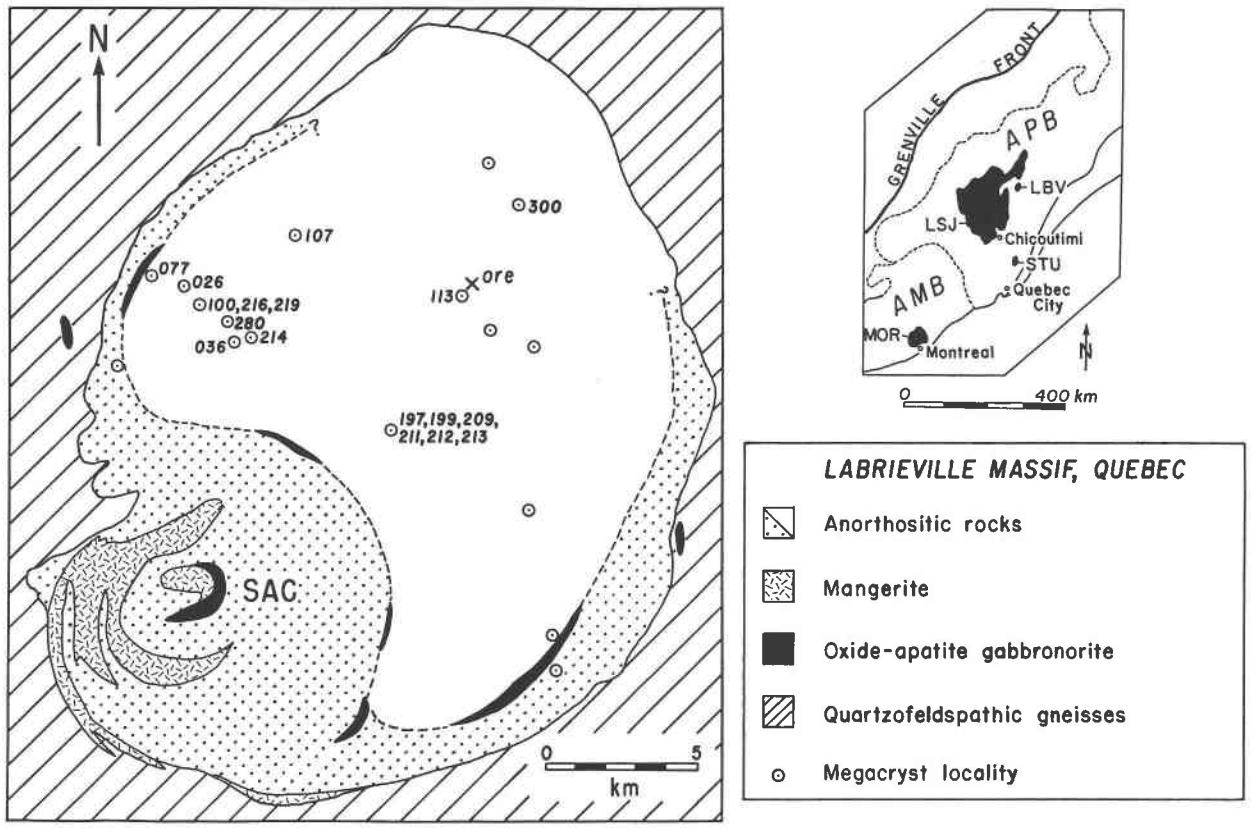

Fig. 1. Sketch map of the Labrieville massif, Quebec. Numbered circles indicate locations of analyzed samples. Unnumbered circles show locations of some additional megacryst sample sites studied petrographically, but megacrysts are not limited to these locations. Anorthositic rocks of the core (unpatterned) include foliated anorthosite and leuconorite, whereas those of the rim (stippled pattern) and the Sault aux Cochons complex (SAC) include relatively massive anorthosite and leucogabbro (see Owens, 1992, and Owens et al., 1994, for additional information). Other abbreviations on index map include AMB (allochthonous monocyclic belt), APB (allochthonous polycyclic belt), MOR (Morin anorthosite), LSJ (Lac Saint Jean anorthosite), STU (Saint Urbain anorthosite), and LBV (Labrieville anorthosite).

tion continues to be attractive (e.g., Goodwin, 1992, p. 389; Ashwal, 1993, p. 141), perhaps because if true, it would provide the only tangible evidence for fractionation of mafic phases at depth, a process demanded by all models deriving massif anorthosite from basalt pooled near the crust-mantle boundary. If, on the other hand, local conditions of crystallization govern the nature of megacrysts and they formed in the outcrops where they now reside, then each suite of OPMs should possess specific features linking them to their host anorthosite. Furthermore, the crystallization sequence inferred from the textures of megacrysts—plagioclase before or after pyroxene—has important implications for the choice of parental magma composition, and the liquid line of descent of that magma.

Geologic setting

The Labrieville massif is located ~325 km north-northeast of Quebec City, within the central granulite terrain of the Grenville structural province (Wynne-Edwards, 1972), or what is now termed the allochthonous polycyclic belt (Rivers et al., 1989). The massif is crudely circular in plan view (Fig. 1) and structurally represents a dome in which the core consists of foliated anorthosite and minor leuconorite and the rim consists of relatively massive leucogabbro and anorthosite. Additional rock types of note include thin units of melanocratic rock known as oxide + apatite gabbronorite (Owens and Dymek, 1992), a small ilmenite ore deposit, and layers and dikes of jotunite (Owens et al., 1993). An extended description of the Labrieville massif and its surroundings appears in Owens et al. (1994), who reported relatively young uranium lead zircon ages of ~1010 Ma for leucogabbro and cogenetic jotunite. Labrieville thus appears to be one of a series of late- to post-tectonic plutons in this region that display no clear evidence of a Grenvillian metamorphic overprint.

Megacryst field relations

Pyroxene megacrysts occur at dozens of localities throughout the Labrieville massif, primarily in core anorthosite, although a few are found in oxide + apatite

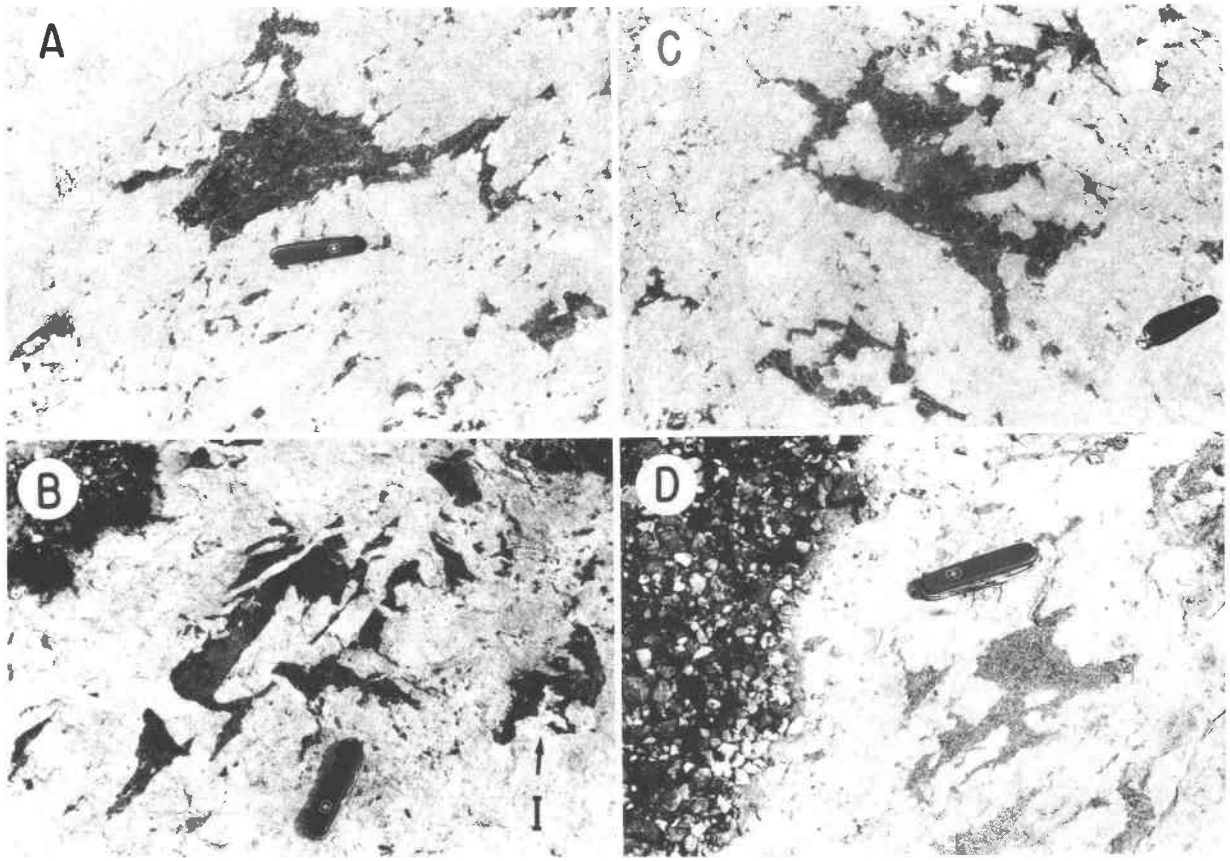

Fig. 2. Field photos of pyroxene megacrysts at Labrieville. (**A**) An aggregate of several OPMs (above knife), each ~10 cm long, in an outcrop containing many smaller pyroxenes. (**B**) A coarse intergrowth of pyroxene megacrysts and tabular plagioclase crystals; area marked I consists of large ilmenite crystals. (**C**) Subophitic intergrowth of orthopyroxene megacrysts and plagioclase; note range in size of pyroxene (dark material). (**D**) Subophitic intergrowth of salt-and-pepper textured plagioclase and orthopyroxene; such features appear to represent recrystallized OPMs.

gabbronorite and border leucogabbro (Fig. 1). Indeed, a common mode of occurrence for pyroxene in this massif is as "megacrysts" (i.e., crystals with plagioclase lamellae, regardless of size). OPMs and CPMs are both present, but OPMs seem to be the more abundant variety (on the basis of current sampling), which is consistent with the overall predominance of orthopyroxene throughout the massif.

Megacrysts appear randomly distributed in most outcrops (Fig. 2A), especially in the flat, glacially polished exposures in the central part of the dome (where the foliation is close to horizontal). In addition, some megacrysts occur within crudely layered zones, which consist of alternations of anorthosite, medium-grained leuconorite, and coarse-grained megacrystic leuconorite. This layering occurs on a scale of several meters, but its lateral extent and continuity cannot be evaluated because of poor exposure. In some of these layered zones, megacrysts appear flattened in the plane of foliation and display variable degrees of recrystallization (see below).

Megacrysts range in size from about a centimeter up to several tens of centimeters across, and in many grains, thin white lamellae (of plagioclase) are observable with the naked eye. Numerous megacrysts show well-developed subophitic textures, and some contain tabular inclusions of plagioclase or plagioclase aggregates (Fig. 2B, 2C). In several outcrops, pyroxene megacrysts occur together with plagioclase megacrysts of similar size and, in most cases, the shapes of pyroxene megacrysts are controlled by adjacent plagioclase crystals (Fig. 2B, 2C).

Pyroxene megacrysts also occur with pods of ilmenite, some of which range up to tens of centimeters across (Fig. 2B). Although these pods now consist of polygonal iron titanium oxide aggregates, they may represent recrystallized larger crystals. The association of pyroxene megacrysts with ilmenite is especially common at Labrieville and, at many localities, both display identical textures. Within individual outcrops, grains of pyroxene and ilmenite span a similar size range (>10 cm down to a few millimeters across), and both form subophitic intergrowths with plagioclase. In addition, pyroxene megacrysts in many cases are intimately intergrown with ilmenite, suggesting that they formed together in place. At one noteworthy locality, about 0.5 km from the ore deposit (Fig. 1), a number of irregularly shaped ilmenite

Fig. 3. Photomicrographs of textures shown by pyroxene megacrysts at Labrieville. (**A**) Typical appearance of plagioclase exsolution lamellae in an OPM. Note how each lamella maintains a nearly constant width across this field of view; also note the additional presence of ilmenite (black) in the thin lamella in the center of the photograph (sample LV91-213; plane-polarized light, horizontal dimension = 2.63 mm). (**B**) Plagioclase lamellae of variable shape and thickness, including a large cluster of plagioclase grains (sample LV90-197; plane-polarized light, horizontal dimension = 2.63 mm). (**C**) Composite lamellae consisting of plagioclase (white), ilmenite (black), and biotite (B) in a typical OPM (sample LV91-213; plane-polarized light, horizontal dimension = 1.32 mm). (**D**) Large OPM (dark, bottom) separated from surrounding plagioclase (white, top) by a layer of biotite (B); also associated with the biotite are grains of hornblende (H) and ilmenite (I), as well as a cluster of apatite crystals (Ap). Such biotite selvages occur with a great number of OPMs (sample LV91-213; plane-polarized light, horizontal dimension = 1.32 mm). (**E**) CPM at extinction, containing a multitude of exsolution lamellae. Bright white lamellae of variable thickness are plagioclase, and the thin lamellae are orthopyroxene; the line points to a coarsened orthopyroxene (Opx) surrounding ilmenite (black), which are intergrown with a coarsened plagioclase (sample LV90-197; cross-polarized light, horizontal dimension = 2.63 mm). (**F**) OPM traversed by two zones of polygonally recrystallized orthopyroxene (O) with minor plagioclase. Thicker bright lamellae (F) are plagioclase, and the thin lamellae are clinopyroxene (sample LV88-036.2; cross-polarized light, horizontal dimension = 2.63 mm).

→

pods (up to ~1 m across) completely enclose pyroxene megacrysts.

A final point of note is the common occurrence, in the same outcrops, of megacrysts with smaller matrix pyroxenes that range in size down to a few millimeters (Fig. 2A). In some cases, it is not possible to distinguish unequivocally such matrix pyroxene from what might be recrystallized megacrysts. The latter have a salt and pepper appearance, consisting of small white plagioclase grains, which we infer to be remnants of lamellae, dispersed among granular clusters of millimeter-sized pyroxene grains without lamellae (Fig. 2D). In general, pyroxene grains ≥0.5 cm across have plagioclase lamellae, and smaller crystals do not.

Megacryst petrography

Orthopyroxene

The most striking petrographic feature of the OPMs is the presence of plagioclase exsolution lamellae oriented parallel to (100) of the host. Most plagioclase lamellae also contain additional segments of ilmenite (Fig. 3A). The ilmenite occurs as small equant inclusions within the plagioclase lamellae (Fig. 3B), or as elongate segments within composite plagioclase + oxide lamellae.

Individual plagioclase lamellae have a relatively constant width (<20 μm up to 200 μm; Fig. 3A), but some show slight thinning and thickening along their lengths; others broaden into larger grains that look like inclusions (Fig. 3B). These features probably represent the migration and coalescence of lamellae material following exsolution and may indicate precipitate coarsening in the sense of Champness and Lorimer (1976). Lamellae spacing is variable, with distances between them in the range 200–800 μm. A few plagioclase lamellae span almost the entire length of their host pyroxene, but most are discontinuous. Many lamellae consist of a single elongate plagioclase grain, but some are made of smaller grains aligned end to end, like beads on a string, probably reflecting some degree of recrystallization (a hint of this texture appears in Fig. 3B). All plagioclase grains in lamellae display albite twinning, with twin composition planes being oriented at any angle to the lamella-host interface. Thicker lamellae show reverse optical zoning.

Most OPMs show minor additional exsolution in the form of platelets of ilmenite on the submicrometer scale and narrow lamellae of clinopyroxene up to a few micrometers wide. These ilmenite and clinopyroxene lamellae occur irregularly throughout the OPMs, with no obvious spatial relationship to the plagioclase lamellae.

Red-brown biotite and green hornblende are also present, typically at megacryst margins (Fig. 3D), but locally penetrating into the OPMs along the length of the plagioclase lamellae (see Fig. 12 of Dymek and Gromet, 1984). In a few cases, biotite occurs as an integral part of the composite plagioclase + oxide lamellae (Fig. 3C) and conceivably is also of exsolution origin. In one OPM, large grains of hornblende occur together with plagioclase in inclusion-like masses up to 2 mm across, along with ilmenite, biotite, and even apatite. In another case, a veinlet, containing small grains of plagioclase and large grains of ilmenite and apatite, crosses an OPM (see Fig. 11 of Dymek and Gromet, 1984). In a few cases, the biotite and hornblende occur in obviously recrystallized areas and may be secondary in origin.

OPMs display variable degrees of recrystallization internally and along their margins. Interiors of several OPMs are traversed by kink bands, which may be decorated with numerous smaller equant pyroxene grains (similar in appearance to Fig. 3F). Many megacrysts are surrounded by a mosaic of equant pyroxene grains and by smaller plagioclase grains that probably represent recrystallized lamellae.

Clinopyroxene

CPMs are similar petrographically in most respects to OPMs in that they contain abundant composite plagioclase + ilmenite lamellae. CPMs have additional coarse lamellae (up to 200 μm wide) of orthopyroxene. These occur both as isolated lamellae and as integral parts of composite lamellae with plagioclase + ilmenite (Fig. 3E).

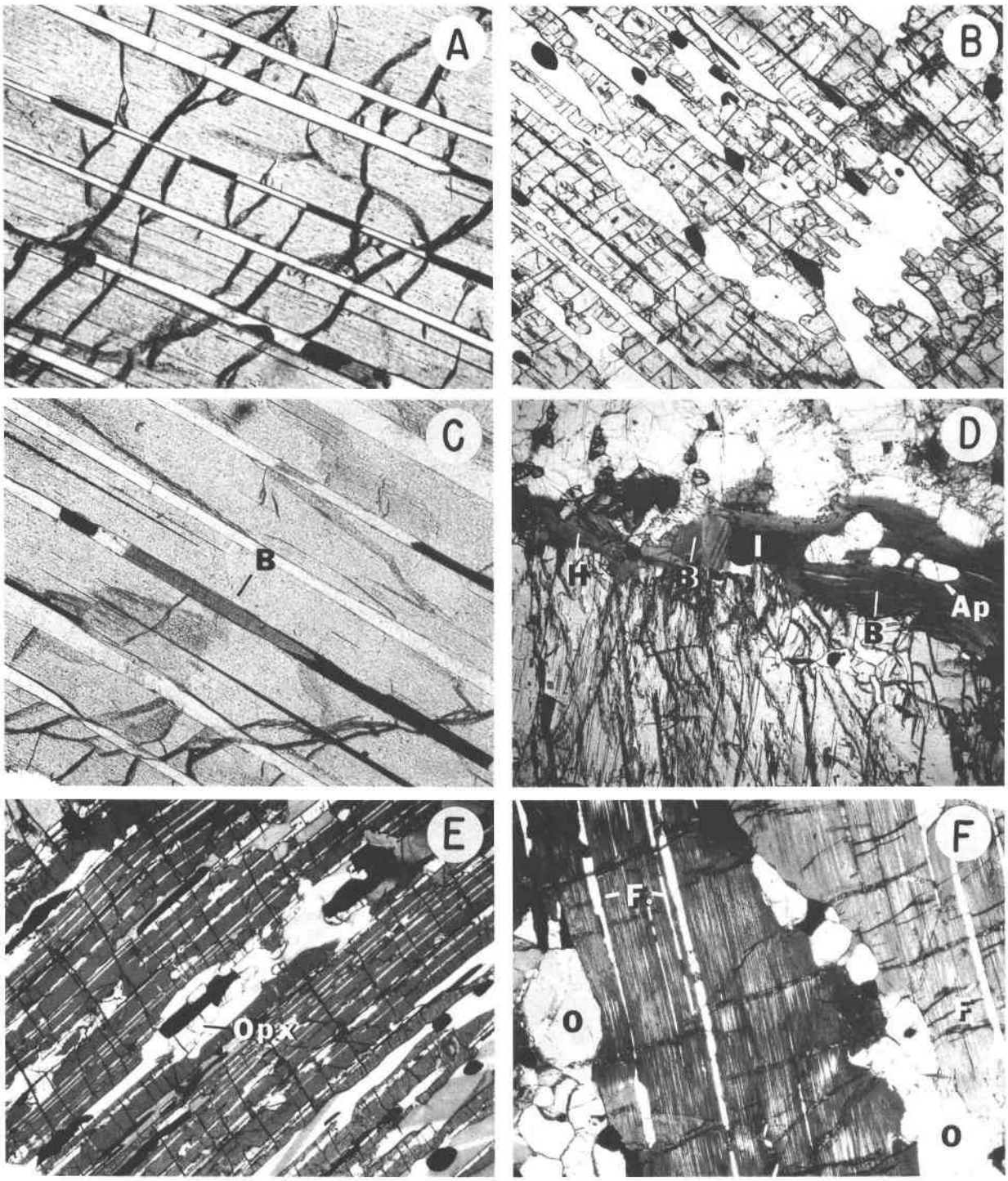

CPMs also contain conspicuous biotite and hornblende, which occur mainly as described above in OPMs.

Matrix pyroxene

Orthopyroxene is the dominant pyroxene throughout the core anorthosite and typically occurs as equant to slightly elongate grains in the size range of 0.5–2.0 mm. Numerous grains contain fine-scaled exsolution lamellae of clinopyroxene, but many are lamella free. On the other hand, nearly all grains contain thin exsolved platelets of ilmenite. Clinopyroxene also occurs throughout the core anorthosite, mainly as small interstitial grains or, rarely,

TABLE 1. Selected spot analyses of pyroxene megacrysts, Labrieville massif

Anal. no.	1	2	3	4	5	6	7	8
Sample	213	212	107	219	211	036	113	100.2
Type	OPM	OPM	OPM	OPM	OPM	OPM	OPM	OPM
SiO_2	52.13	53.01	52.06	52.58	52.99	52.42	51.74	51.40
TiO_2	0.13	0.11	0.09	0.11	0.13	0.11	0.14	0.12
Al_2O_3	2.48	2.00	1.74	1.76	2.27	1.66	2.06	1.94
Cr_2O_3	0.00	0.00	0.00	0.00	0.00	0.01	0.01	0.01
FeO	20.54	20.83	21.73	22.81	20.42	22.19	21.63	23.30
MnO	0.37	0.41	0.37	0.41	0.54	0.38	0.51	0.44
MgO	23.80	22.91	22.95	21.85	23.34	22.74	23.12	21.65
CaO	0.66	0.54	0.46	0.72	0.53	0.66	0.61	0.58
Na_2O	0.03	0.02	0.01	0.01	0.02	0.02	0.02	0.02
Total	100.14	99.83	99.41	100.25	100.24	100.19	99.84	99.46
Formula proportions based on 4 cations and 6 O atoms								
Si	1.915	1.964	1.939	1.956	1.950	1.942	1.917	1.929
$^{[4]}Al$	0.085	0.036	0.061	0.044	0.050	0.058	0.083	0.071
$^{[6]}Al$	0.022	0.051	0.016	0.033	0.049	0.014	0.007	0.015
Cr	0.000	0.000	0.000	0.000	0.000	0.000	0.000	0.000
Fe^{3+}	0.057	0.000	0.041	0.005	0.000	0.039	0.069	0.050
Ti	0.004	0.003	0.003	0.003	0.004	0.003	0.004	0.003
Mg	1.303	1.265	1.274	1.212	1.280	1.256	1.277	1.211
Mn	0.012	0.013	0.012	0.013	0.017	0.012	0.016	0.014
Fe^{2+}	0.574	0.645	0.636	0.705	0.628	0.648	0.601	0.681
Ca	0.026	0.021	0.018	0.029	0.021	0.026	0.024	0.023
Na	0.002	0.001	0.001	0.001	0.001	0.001	0.001	0.001
End-member proportions in atomic percent								
Ca	1.3	1.1	0.9	1.5	1.1	1.3	1.2	1.2
Mg	66.1	65.1	64.3	61.7	65.8	63.4	64.3	61.2
Fe + Mn	32.6	33.8	34.8	36.8	33.1	35.3	34.5	37.6

Note: electron microprobe methods described in Owens and Dymek (1992).

TABLE 2. Selected spot analyses of non-megacrystic pyroxene, Labrieville massif

Anal. no.	1	2	3	4	5	6	7	8	9	10	11	12
Sample	201	219	220	099	036	106	197	106	122	215	209	199
Type	opx	opx	opx	opx	opx	opx	cpx	cpx	cpx	cpx	cpx	cpx
SiO_2	52.15	52.73	52.44	51.82	52.39	51.72	51.45	50.79	50.85	51.45	50.68	51.07
TiO_2	0.22	0.11	0.13	0.17	0.13	0.15	0.42	0.49	0.47	0.64	0.57	0.54
Al_2O_3	1.30	1.42	1.26	1.46	1.38	1.41	2.78	2.76	2.61	2.73	3.60	3.47
Cr_2O_3	0.00	0.00	0.04	0.03	0.00	0.00	0.00	0.00	0.00	0.00	0.01	0.02
FeO	21.99	23.18	24.18	23.57	23.94	23.76	9.91	9.49	9.69	9.55	9.33	8.61
MnO	0.34	0.40	0.55	0.46	0.41	0.75	0.27	0.24	0.31	0.27	0.25	0.28
MgO	22.83	21.93	24.18	21.71	21.58	21.51	13.15	13.39	12.83	12.51	13.03	13.08
CaO	0.66	0.49	0.71	0.74	0.50	0.47	21.36	21.86	22.46	21.99	21.23	22.59
Na_2O	0.01	0.00	0.01	0.03	0.00	0.01	0.69	0.62	0.65	0.64	0.76	0.76
Total	99.50	100.26	99.41	100.01	100.33	99.78	100.03	99.64	99.87	99.78	99.46	100.42
Formula proportions based on 4 cations and 6 O atoms												
Si	1.944	1.963	1.970	1.937	1.955	1.941	1.916	1.896	1.889	1.927	1.894	1.888
$^{[4]}Al$	0.056	0.037	0.030	0.063	0.045	0.059	0.084	0.104	0.101	0.073	0.106	0.112
$^{[6]}Al$	0.002	0.026	0.026	0.001	0.016	0.003	0.039	0.018	0.014	0.047	0.053	0.039
Cr	0.000	0.000	0.001	0.001	0.000	0.000	0.000	0.000	0.000	0.000	0.000	0.001
Fe^{3+}	0.042	0.005	0.000	0.054	0.022	0.048	0.071	0.103	0.107	0.036	0.076	0.096
Ti	0.006	0.003	0.004	0.005	0.004	0.004	0.012	0.014	0.013	0.018	0.016	0.015
Mg	1.269	1.217	1.163	1.209	1.200	1.203	0.730	0.745	0.714	0.698	0.726	0.721
Mn	0.011	0.013	0.018	0.015	0.013	0.024	0.009	0.008	0.010	0.009	0.008	0.009
Fe^{2+}	0.643	0.717	0.760	0.683	0.725	0.698	0.237	0.193	0.195	0.263	0.216	0.170
Ca	0.026	0.020	0.029	0.030	0.020	0.019	0.852	0.874	0.899	0.882	0.850	0.895
Na	0.001	0.000	0.000	0.002	0.000	0.001	0.050	0.045	0.047	0.046	0.055	0.054
End-member proportions in atomic percent												
Ca	1.3	1.0	1.4	1.5	1.0	1.0	44.9	45.5	46.7	46.7	45.3	47.3
Mg	63.7	61.7	59.1	60.7	60.6	60.4	38.4	38.7	37.1	37.0	38.7	38.1
Fe + Mn	35.0	37.3	39.5	37.8	38.4	38.6	16.7	15.8	16.2	16.3	16.0	14.5

Note: locations of samples not shown on Fig. 1 appear on Fig. 5.2 in Owens (1992).

TABLE 1.—*Continued*

Anal no.	9	10	11	12	13	14	15	16	17
Sample	100.3	216	026	077	214	197	211	209	199
Type	OPM	OPM	OPM	OPM	CPM	CPM	CPM	CPM	CPM
SiO_2	52.36	51.88	51.59	51.58	52.17	51.33	50.72	50.68	51.07
TiO_2	0.11	0.12	0.12	0.11	0.36	0.38	0.63	0.57	0.54
Al_2O_3	1.75	1.88	2.11	1.41	2.82	2.76	4.11	3.60	3.47
Cr_2O_3	0.05	0.00	0.03	0.01	0.03	0.00	0.05	0.01	0.02
FeO	22.99	22.89	22.32	25.30	8.78	9.70	8.73	9.33	8.61
MnO	0.44	0.40	0.38	0.58	0.26	0.29	0.25	0.25	0.28
MgO	21.91	22.54	22.26	20.36	13.85	13.69	13.12	13.03	13.08
CaO	0.87	0.35	0.48	0.57	21.39	21.42	21.43	21.23	22.59
Na_2O	0.02	0.01	0.02	0.01	0.62	0.68	0.72	0.76	0.76
Total	100.50	100.07	99.31	99.93	100.28	100.25	99.76	99.46	100.42
Formula proportions based on 4 cations and 6 O atoms									
Si	1.943	1.928	1.930	1.947	1.930	1.903	1.887	1.894	1.888
$^{[4]}Al$	0.057	0.072	0.070	0.053	0.070	0.097	0.113	0.106	0.112
$^{[6]}Al$	0.020	0.010	0.023	0.010	0.053	0.023	0.067	0.053	0.039
Cr	0.001	0.000	0.001	0.000	0.001	0.000	0.001	0.000	0.001
Fe^{3+}	0.031	0.057	0.040	0.037	0.040	0.101	0.061	0.076	0.096
Ti	0.003	0.003	0.003	0.003	0.010	0.011	0.018	0.016	0.015
Mg	1.212	1.248	1.241	1.146	0.764	0.756	0.728	0.726	0.721
Mn	0.014	0.013	0.012	0.019	0.008	0.009	0.008	0.008	0.009
Fe^{2+}	0.683	0.655	0.658	0.762	0.231	0.199	0.211	0.216	0.170
Ca	0.035	0.014	0.019	0.023	0.848	0.851	0.854	0.850	0.895
Na	0.001	0.001	0.001	0.001	0.044	0.049	0.052	0.055	0.054
End-member proportions in atomic percent									
Ca	1.8	0.7	1.0	1.2	44.8	44.4	45.9	45.3	47.3
Mg	61.4	62.8	63.0	57.7	40.4	39.5	39.1	38.7	38.1
Fe + Mn	36.9	36.5	36.0	41.2	14.8	16.1	15.0	16.0	14.5

as thin, partial rims on orthopyroxene or ilmenite. Such clinopyroxene grains show no exsolution features.

CHEMICAL COMPOSITIONS

Spot analyses of pyroxenes

Selected spot analyses from 12 OPMs and five CPMs, as determined by electron microprobe methods, are listed in Table 1. These data are representative of megacryst compositions away from any obvious exsolution lamellae. For purposes of comparison, selected spot analyses of non-megacrystic (non-lamella-bearing) pyroxene from throughout the Labrieville massif are listed in Table 2.

OPM and CPM spot compositions from Table 1 are illustrated on a pyroxene quadrilateral in Figure 4. OPMs in anorthosite and leuconorite span a narrow compositional range from En_{66} to En_{61}, whereas a single OPM from oxide + apatite gabbronorite is slightly more Fe-rich at En_{58}. CPM spot analyses cluster near $Ca_{45}Mg_{40}Fe_{15}$. These compositions overlap almost completely the fields of other ortho- and clinopyroxenes throughout the massif, represented by the stippled fields on Figure 4.

The concentrations of Al_2O_3, TiO_2, MnO, and Na_2O in OPMs and CPMs show some variation, both within and between megacrysts, but there is no clear correlation with X_{Mg} (Figs. 5 and 6). Spot compositions of CPMs are distinguished from OPMs by higher X_{Mg}, Al_2O_3, TiO_2, and Na_2O, but lower MnO. Levels of Cr in both types are at or below detection limits of the electron microprobe (<0.05 wt% Cr_2O_3). In some megacrysts, concentrations of minor elements are lower in rims than cores, which may be evidence for relic zoning. Similarly, there is a slight drop in Al adjacent to plagioclase lamellae in a few cases, although for the most part, variations within the megacryst are not obviously related to proximity to exsolution lamellae.

Compared with the compositions of other pyroxenes in the massif, spot compositions from OPMs and CPMs show a broad region of overlap, both in terms of X_{Mg} and concentrations of minor elements (Figs. 5 and 6). Thus, the process of plagioclase and ilmenite exsolution in megacrysts yields residual pyroxene compositions that closely resemble other pyroxenes in the Labrieville massif (cf. Fig. 4).

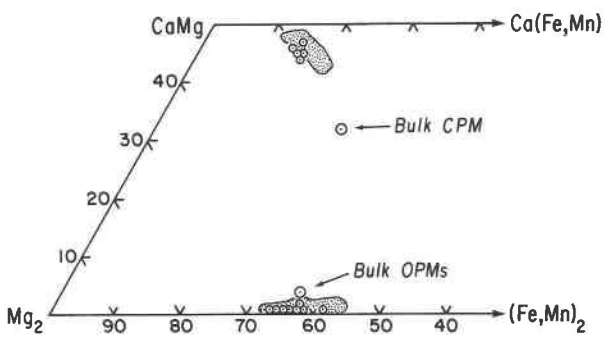

Fig. 4. Quadrilateral plot of spot compositions in pyroxene megacrysts and bulk compositions of three OPMs (all of which plot at the same point) and one CPM. Stippled fields encompass data points for other pyroxenes throughout the massif (Owens, 1992).

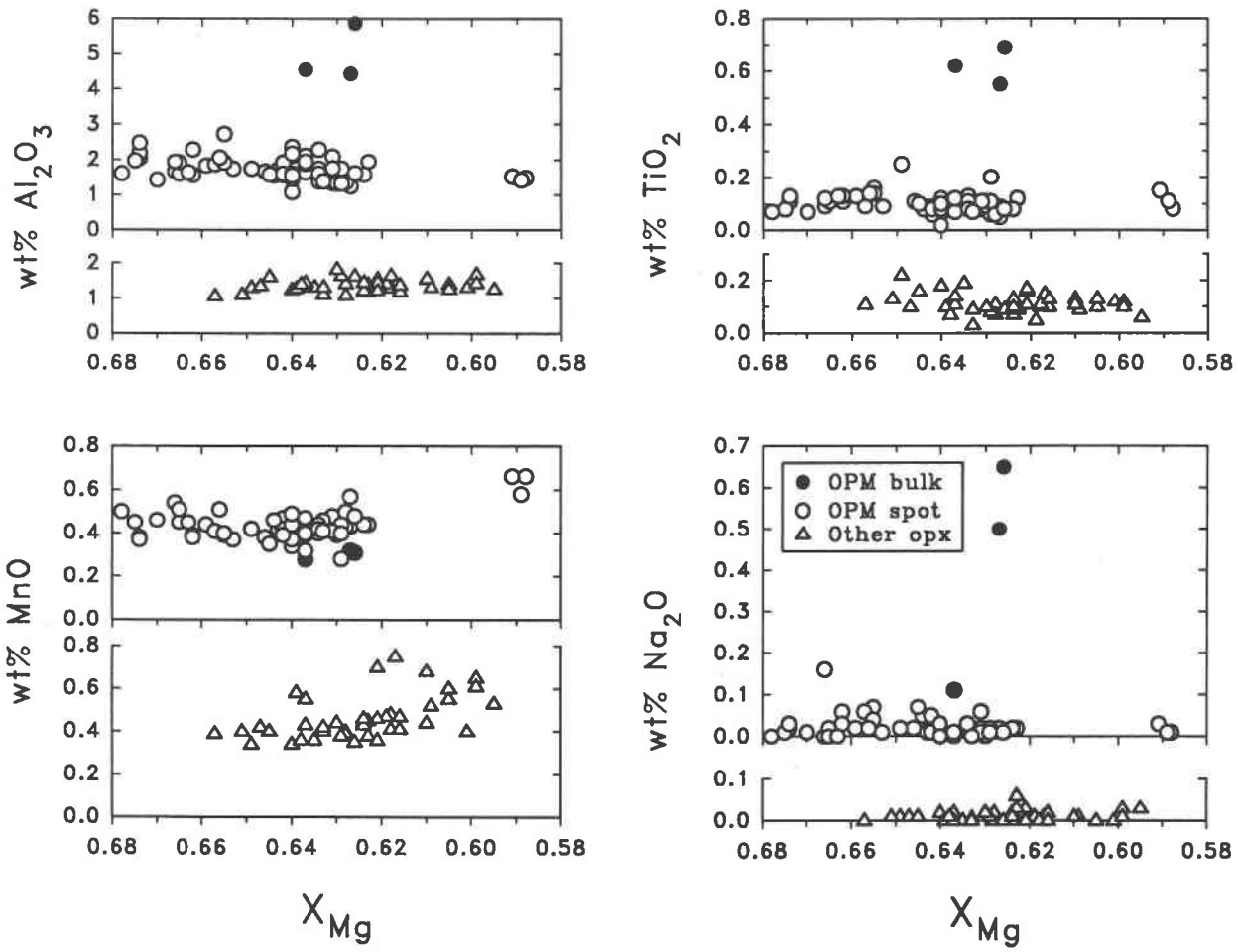

Fig. 5. Plots of wt% Al_2O_3, TiO_2, MnO, and Na_2O vs. X_{Mg} [=Mg/(Mg + Fe_{tot})] for spot and bulk compositions of orthopyroxene megacrysts, and other orthopyroxene in the massif.

Bulk analyses of pyroxenes

Three OPMs and one CPM (each ~5 cm across) were selected for bulk-chemical analysis. Care was taken during sample preparation to remove any matrix material adhering to the margins of the megacrysts, so that only interiors were analyzed. Results for major and trace elements, as determined by XRF methods, are given in Table 3. For comparison, the bulk compositions of four OPMs from Saint Urbain (Dymek and Gromet, 1984), including new XRF trace element analyses, are presented in Table 4.

In each case, recalculated compositions yielded reasonable pyroxene stoichiometry, in which the majority of the Al occurs in tetrahedral sites. In terms of quadrilateral components, the bulk OPMs differ little from other orthopyroxenes in the massif, apart from containing slightly higher Ca (Fig. 4). This higher Ca primarily reflects the presence of the plagioclase lamellae in reconstituted OPMs, since clinopyroxene exsolution is of only minor importance. Bulk OPMs fall within the range defined by other orthopyroxenes for X_{Mg} (Fig. 5). However, bulk OPMs are enriched in Al_2O_3 (~4.4–5.9 wt%), TiO_2 (~0.55–0.69 wt%), and Na_2O (up to 0.65 wt%) relative to spot compositions and other orthopyroxene in the massif (Fig. 5); we note that Al and Ti correlate positively (Table 3). Bulk compositions appear slightly lower in MnO relative to spot compositions, probably reflecting an enrichment of MnO in residual pyroxene due to plagioclase and ilmenite exsolution. Amounts of exsolution products, calculated by the least-squares approximation method of Bryan et al. (1969), are ~9 wt% plagioclase, ~4 wt% ilmenite, and negligible clinopyroxene.

Compared with the bulk OPMs, the bulk CPM contains more Al_2O_3 (~6.4 wt%), TiO_2 (~1.2 wt%), and Na_2O (~1.3 wt%), but a similar amount of MnO (~0.3 wt%). Compared with CPM spot compositions and other clinopyroxenes in the massif (Fig. 6), the bulk CPM is also enriched in Na, Al, and Ti (but has similar Mn). Most notably, the bulk CPM is substantially enriched in Fe and depleted in Ca compared with all other clinopyroxene compositions, as indicated by its location on the pyroxene quadrilateral (Figs. 4 and 6). This compositional shift

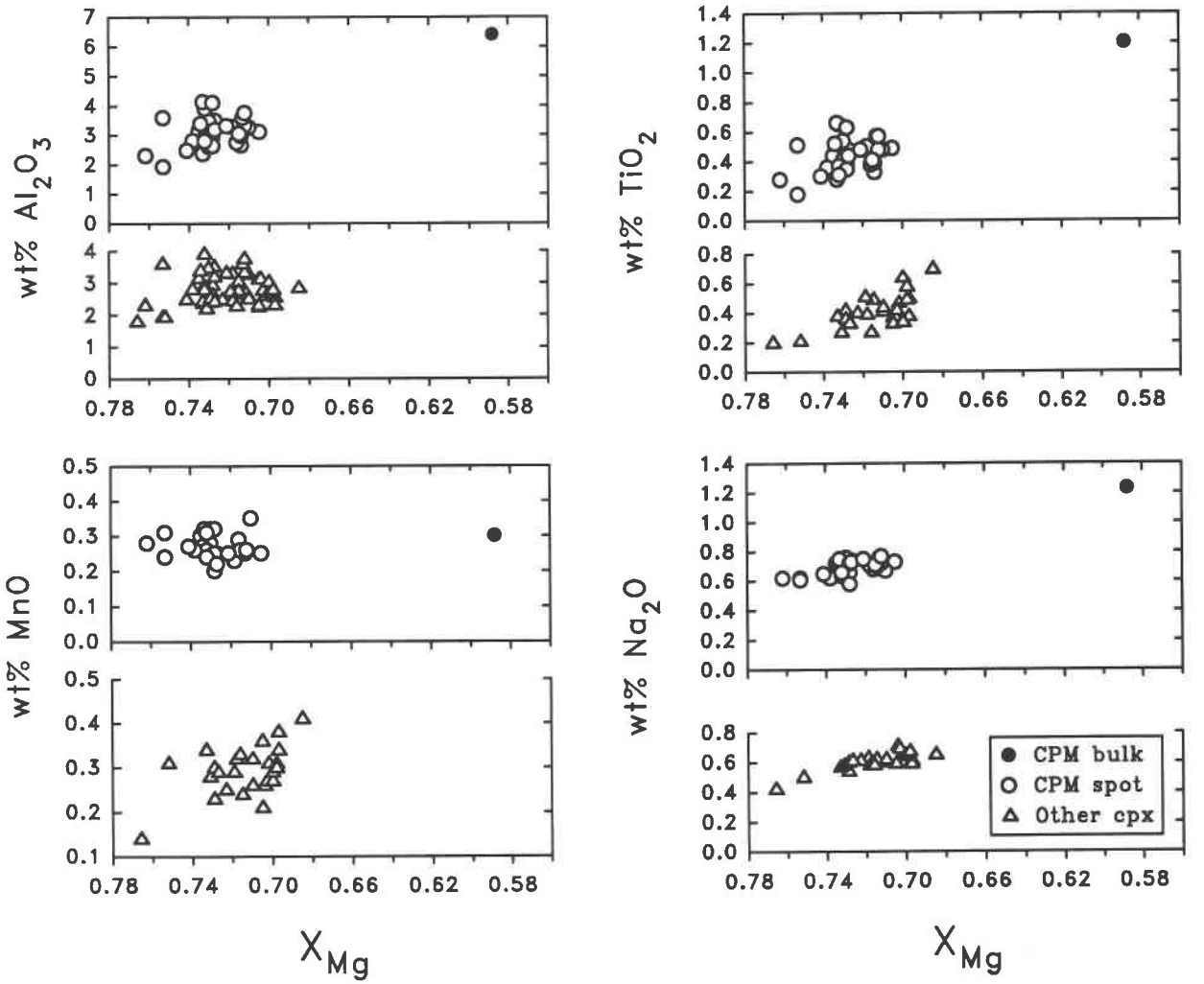

Fig. 6. Plots of wt% Al_2O_3, TiO_2, MnO, and Na_2O vs. X_{Mg} [=Mg/(Mg + Fe_{tot})] for spot and bulk compositions of clinopyroxene megacrysts, and other clinopyroxene in the massif.

reflects the presence of ~7 wt% exsolved ilmenite and ~22 wt% exsolved orthopyroxene (plus ~13 wt% plagioclase, calculated by least squares approximation). Thus, the CPM consists by weight of >40% exsolution products.

The OPMs contain variable V (~150–220 ppm) and Cr (~100–380 ppm); it is noteworthy that the OPM with the highest Al also has the highest V and Cr (and Ga). Concentrations of Ni (~115–150 ppm) and Co (~100 ppm) are lower and less variable, whereas Zn is uniformly higher (~325–350 ppm). Sr (9–40 ppm), Y (~7 ppm), and Zr (~25 ppm) are all low, as is Ba, although the amount found in OPM no. 280 (67 ppm) seems anomalously high. Compared with the OPMs, the CPM contains higher Sr, Y, Zr, and V, but lower Cr, Co, Ni, and Zn.

Compared with bulk compositions of OPMs from Saint Urbain (Table 4), those from Labrieville are more Fe-rich (~21.3–21.8 vs. ~19.5–20.2 wt% FeO_{tot}). Labrieville OPMs have similar Al_2O_3 and TiO_2, slightly higher CaO and MnO, and significantly higher Na_2O (apart from sample no. 300). The Labrieville OPMs contain higher Zn, Sr, Y, and Zr, similar Ga, lower V and Co, and substantially lower Cr and Ni.

Compositions of plagioclase lamellae

Selected analyses of plagioclase lamellae from OPMs and CPMs are listed in Table 5 and illustrated in histogram form in Figure 7. Compositions of lamellae in OPMs range from An_{38} to An_{53}, with a peak at An_{46}. In contrast, lamellae in CPMs are typically more albitic, with a peak at An_{39} (apart from sample no. 211, in which lamellae range up to ~An_{50}). Individual lamellae in both types of megacrysts show little change in composition along their lengths, and lamellae compositions are relatively constant throughout a single megacryst. However, analyses do confirm the reverse zoning detected optically, with measured compositions varying by up to ~5 mol% An in thicker lamellae.

TABLE 3. Bulk compositions of Labrieville pyroxene megacrysts

Sample	107	280	300	209
Type	OPM	OPM	OPM	CPM
SiO_2	49.98	48.89	50.14	48.04
TiO_2	0.55	0.69	0.62	1.20
Al_2O_3	4.41	5.86	4.53	6.40
$Fe_2O_{3\,tot}$	23.95	23.37	23.68	17.02
MnO	0.32	0.31	0.29	0.30
MgO	20.04	19.73	20.97	12.25
CaO	1.59	1.65	1.40	13.87
Na_2O	0.42	0.65	0.11	1.23
K_2O	0.07	0.08	0.08	0.09
P_2O_5	0.03	0.02	0.03	0.19
LOI	−0.97	−0.08	−0.64	−0.14
Total	100.40	101.18	101.22	100.45
V	148	218	176	242
Cr	101	353	95	45
Co	99	102	103	65
Ni	115	120	150	52
Cu	<12	n.a.	n.a.	<12
Zn	348	350	324	182
Ga	13.6	16.4	14.1	16.1
Rb	<3.3	<3.3	<3.3	<3.0
Sr	40	27	9	158
Y	6.2	5.8	7.0	23.5
Zr	26	23	19	68
Nb	<3	<3	<3	<2
Ba	<18	67	29	68
Ce	<19	<19	<20	<21
Sn	<7	<7	<7	<7
Pb	<10	<7	<14	<8
	Formula proportions*			
Si	1.881	1.834	1.875	1.829
$^{[4]}Al$	0.119	0.166	0.125	0.171
$^{[6]}Al$	0.077	0.094	0.075	0.116
Fe^{3+}	0.041	0.080	0.024	0.077
Ti	0.016	0.020	0.017	0.034
Mg	1.124	1.104	1.169	0.695
Mn	0.010	0.010	0.009	0.010
Fe^{2+}	0.638	0.579	0.643	0.411
Ca	0.064	0.066	0.056	0.566
Na	0.030	0.047	0.008	0.091

Note: major elements in weight percent, trace elements in parts per million; XRF methods described in Owens and Dymek (1992) and Couture et al. (1993); n.a. = not analyzed.

* Formula proportions calculated from bulk analyses normalized to 100% using all Fe as FeO, with K_2O and P_2O_5 ignored.

TABLE 4. Bulk compositions of Saint Urbain pyroxene megacrysts

Sample	CHV80-33	CHV80-33	CHV80-33	CHV80-99
Crystal	OPM A	OPM B	OPM C	OPM A
SiO_2	49.08	49.07	49.67	49.33
TiO_2	0.676	0.687	0.756	0.785
Al_2O_3	4.89	5.10	5.02	5.32
FeO_{tot}	20.22	19.84	20.09	19.54
MgO	23.42	23.53	22.44	23.28
MnO	0.216	0.235	0.245	0.216
CaO	1.28	1.35	1.46	1.27
Na_2O	0.127	0.098	0.186	0.177
Total	99.91	99.91	99.87	99.92
V	185	189	192	200
Cr	749	777	673	567
Ni	321	335	311	371
Co	120	124	118	131
Cu	<11	<11	<11	<11
Zn	213	209	218	199
Ga	13.4	13.9	14.0	14.8
Rb	1.7	<3.0	<3.0	<2.5
Sr	9.5	8.2	11.3	17.1
Y	3.2	2.7	2.9	3.9
Zr	7.7	6.2	8.6	16.8
Nb	1.4	2.6	3.9	4.4
Ba	<19	<19	<19	<15
Pb	<10	<8	<7	<8

Note: major elements in weight percent by electron microprobe analyses on fused glass beads (Table 4 in Dymek and Gromet, 1984); trace elements in parts per million by XRF analyses of pressed powder pellets (this study).

Plagioclase lamellae in both OPMs and CPMs are typically more calcic than other plagioclase in the massif, which shows a strong compositional peak at An_{35} (Fig. 7). This contrast between matrix and lamellar plagioclase compositions is a characteristic feature of all occurrences of pyroxene megacrysts described from other anorthosite massifs. However, the compositions of plagioclase lamellae at Labrieville are the most albitic of any occurrence yet reported.

DISCUSSION

An in-situ origin for pyroxene megacrysts at Labrieville

Field evidence. At least four features suggest an in-situ origin for the OPMs. First, numerous OPMs display unambiguous subophitic textures (Fig. 2), indicating that they grew together with (or after) adjacent grains of plagioclase. Such OPMs could not have crystallized early (before plagioclase) from the magma that produced the anorthosite. Second, in numerous outcrops, megacrysts of plagioclase and large masses of ilmenite occur together with OPMs (Fig. 2). There is no indication (e.g., resorbed cores) that the OPMs formed in an environment different from that in which the plagioclase megacrysts or ilmenite masses formed. Third, the ilmenite masses typically display textures that are similar to those of the pyroxene megacrysts. Furthermore, the widespread occurrence of pyroxene + ilmenite intergrowths indicates cocrystallization of these minerals. Finally, many OPMs occur within crudely layered, pyroxene-rich zones. As argued by Morse (1975), such layered rocks probably originated through local nucleation and growth and accumulation of plagioclase and pyroxene.

Compositional evidence. It is principally the concentrations of minor elements (e.g., Al, Ti, Ca, and Na) that distinguish bulk OPMs from other orthopyroxenes in the massif (Fig. 5). Otherwise, bulk megacrysts are slightly more Fe-rich than associated matrix pyroxene and thus do not appear to be an earlier phase (see later discussion). The striking difference in composition for the bulk CPM relative to other clinopyroxenes in the massif (Figs. 4 and 6) is a feature that we do not understand completely at present. However, this crystal shows even lower X_{Mg} than the bulk OPMs and likewise cannot be considered to have formed early. Our current thinking is that the CPM represents an extreme case of metastable growth, a hypothesis that is consistent with the abundance of coarsely exsolved plagioclase, orthopyroxene, and ilmenite.

Spot compositions of both OPMs and CPMs are the same as for other pyroxene compositions in the massif, not only for X_{Mg}, but also for Al_2O_3, TiO_2, MnO, and Na_2O (Figs. 5 and 6). Thus, spot analyses of megacrysts,

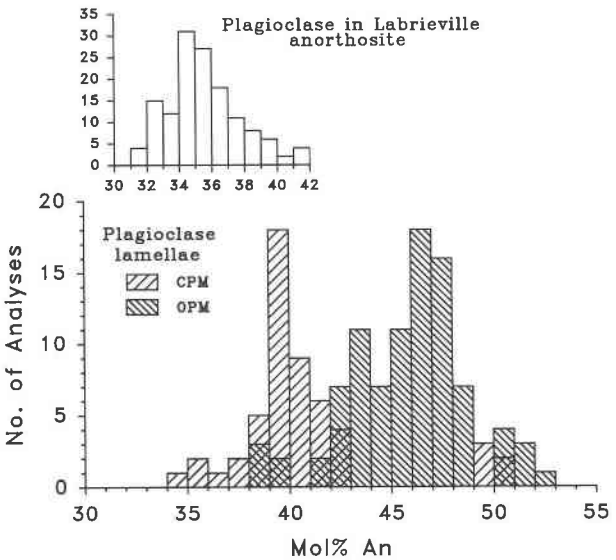

Fig. 7. A histogram of compositions of plagioclase lamellae in pyroxene megacrysts. Compositions of plagioclase in Labrieville anorthositic rocks included for comparison (Owens, 1992). Plagioclase lamellae in megacrysts are typically more calcic than plagioclase in the anorthosite.

although recording post-exsolution compositions, also provide a link with the local environment.

An in-situ origin for megacrysts is also supported by a comparison of the Labrieville and Saint Urbain data sets. In Figure 8 we have plotted X_{Mg} in orthopyroxene and mol% An in plagioclase lamellae of Labrieville and Saint Urbain OPMs and compared these compositions with orthopyroxene and plagioclase in the surrounding matrix of each sample. Figure 8 top confirms that megacrysts and matrix pyroxenes have similar values of X_{Mg}. However, OPMs and matrix pyroxene from Labrieville are both more Fe-rich than their counterparts from Saint Urbain. Figure 8 bottom shows that plagioclase lamellae in OPMs and plagioclase in matrix anorthosite at Labrieville are both more albitic than those at Saint Urbain.

We consider these systematic compositional differences in matrix and megacryst pyroxene, as well as in matrix and lamellae plagioclase, between Saint Urbain and Labrieville to be strong evidence for control by local magma composition. Thus, the more Fe-rich OPMs at Labrieville and their more Na-rich plagioclase lamellae can be explained simply by the growth of megacrysts in a more Fe- and Na-rich environment, i.e., the local anorthosite. In addition, the systematic trace-element differences displayed by OPMs from the two massifs (higher Zn, Y, and Zr, but lower Co, Cr, and Ni in those from Labrieville; Table 4) are consistent with the more evolved nature of Labrieville relative to Saint Urbain.

Implications of in-situ growth for mechanisms of minor element enrichment

Our principal conclusion, that pyroxene megacrysts at Labrieville grew in place, naturally leads us to consider

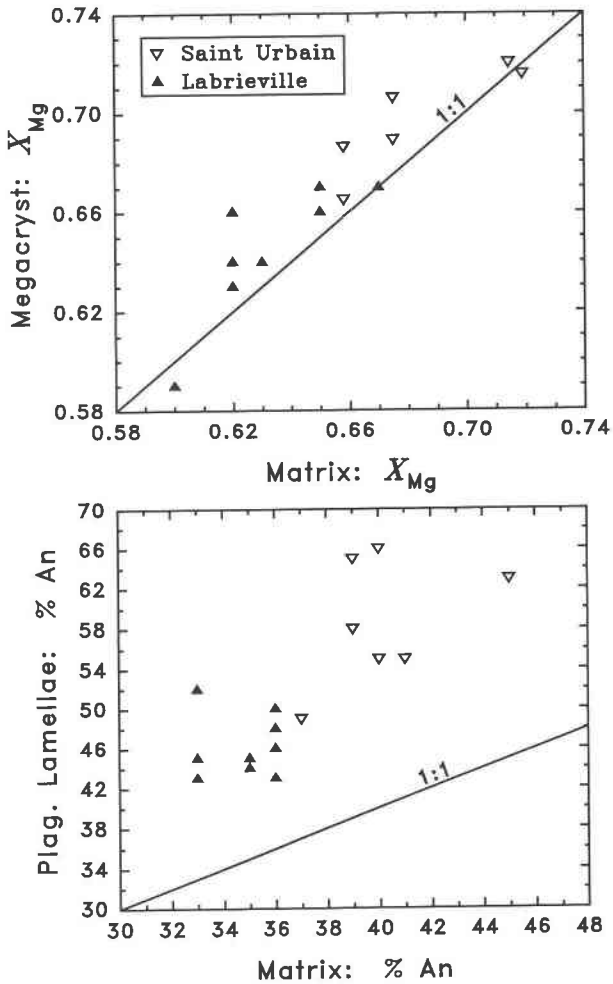

Fig. 8. Plots comparing average spot compositions of orthopyroxene megacrysts, plagioclase lamellae, and matrix minerals at Labrieville and Saint Urbain. The **top** plot shows that both megacryst and matrix pyroxene at Saint Urbain are more magnesian than at Labrieville. The **bottom** plot shows that both lamellae and matrix plagioclase are more calcic than at Labrieville. The 1:1 lines are for reference only.

why they display such unusual petrographic and compositional features. The fact that such megacrysts are apparently restricted to massif anorthosites is, in our opinion, significant and suggests to us that distinctive and possibly unique conditions of crystallization characterize these igneous rocks. Indeed, the petrographic features reported here and in Dymek and Gromet (1984), together with the detailed microstructural observations (TEM and XRD) of Veblen and Bish (1988) on an OPM from the Nain Complex, Labrador, indicate that these megacrysts are complex composite crystals: they contain extensive exsolution lamellae of a wide variety of silicate and oxide minerals, including plagioclase, hornblende, augite, magnetite, hercynite, biotite, and other hybrid lamellae. This diversity of exsolution products is testament to the enhanced incorporation of both nonquadrilateral and non-

TABLE 5. Selected compositions of plagioclase lamellae in Labrieville pyroxene megacrysts

Anal. no.	1	2	3	4	5	6	7	8
Sample	213	212	107	219	211	036	113	100.2
Host	OPM	OPM	OPM	OPM	OPM	OPM	OPM	OPM
SiO_2	56.21	57.03	56.56	55.90	54.44	56.05	56.40	55.81
Al_2O_3	28.03	27.25	27.89	28.02	29.02	27.92	27.91	28.26
FeO	0.28	0.15	0.24	0.37	0.44	0.39	0.29	0.26
CaO	9.72	8.77	9.29	9.76	10.43	9.27	9.17	9.54
Na_2O	5.93	6.21	6.04	5.72	5.14	6.05	5.96	5.84
K_2O	0.36	0.52	0.33	0.42	0.27	0.28	0.26	0.42
BaO	0.01	0.06	0.00	0.02	0.02	0.05	0.00	0.00
Total	100.54	99.99	100.35	100.21	99.76	100.01	99.99	100.13
Formula proportions based on 8 O atoms								
Si	2.518	2.561	2.533	2.513	2.462	2.522	2.533	2.509
Al	1.480	1.442	1.472	1.485	1.547	1.481	1.477	1.497
Fe	0.010	0.006	0.009	0.014	0.017	0.015	0.011	0.010
Ca	0.466	0.422	0.446	0.470	0.505	0.447	0.441	0.460
Na	0.515	0.541	0.524	0.499	0.451	0.528	0.519	0.509
K	0.021	0.030	0.019	0.024	0.016	0.016	0.015	0.024
Ba	0.000	0.001	0.000	0.000	0.000	0.001	0.000	0.000
Total	5.010	5.003	5.003	5.005	4.998	5.010	4.996	5.009
Mol% An	46.5	42.5	45.1	47.3	52.0	45.1	45.3	46.3

pyroxene components into the growing pyroxene crystals.

These observations are consistent with the local nucleation of megacrysts at high temperature, followed by relatively rapid growth, a hypothesis first suggested by Morse (1975) and developed more fully by Dymek and Gromet (1984). Briefly stated, this model calls for the metastable incorporation of excess components in OPMs as a consequence of local supersaturation in pyroxene, leading to accelerated growth. In support of this interpretation, we note the substantial body of data on lunar pyroxene phyric basalts. The lunar analogue is appropriate because a similar debate was carried on regarding near-surface vs. intratelluric crystallization of phenocrysts compared with matrix pyroxene (see review by Dowty et al., 1974). The aluminous nature of zoned lunar phenocrysts was interpreted by some (Bence et al., 1971) to reflect a high-pressure stage of crystallization (analogous to high-pressure growth of OPMs), followed by growth of less-aluminous groundmass pyroxene at low pressure. However, the alternative interpretation (Hollister and Hargraves, 1970; Hollister et al., 1971), that the porphyritic texture of the lunar rocks and the chemical compositions of pyroxenes could be explained by a single episode of continuous crystallization (analogous to in-situ growth of OPMs), was subsequently confirmed by controlled cooling rate experiments (e.g., Lofgren et al., 1974).

Two observations from the lunar studies are particularly relevant to our model for the formation of OPMs. First, pyroxenes (augite or pigeonite) produced in cooling rate experiments (i.e., at elevated growth rates) are enriched at Al, Ti, and Cr relative to those produced in equilibrium experiments (Grove and Bence, 1977, 1979; Grove and Raudsepp, 1978; Shimizu, 1983). These results confirm that rapid growth can lead to elevated concentrations of all minor elements. Second, pyroxene phenocrysts in both natural and experimental samples, although zoned, invariably contain higher concentrations of all minor elements (Al, Ti, and Cr) relative to groundmass pyroxene (Bence et al., 1970; Weill et al., 1971; Lofgren et al., 1974; Grove and Bence, 1977). This enhanced partitioning of Al, Ti, and Cr into rapidly grown lunar pyroxene was attributed by Grove and Bence (1979, p. 465) to "the inability of Al_2O_3 to leave the pyroxene/liquid interface by diffusion through the residual liquid. . .thus, Al is included in growing pyroxene and snatches Ti and Cr from the surrounding residual liquid to balance charge." The fact that OPMs are similarly enriched in minor elements is thus entirely consistent with a rapid growth rate.

The sparse distribution of megacrysts and their large size suggest a lower nucleation rate coupled with a higher growth rate compared with matrix pyroxene (Dowty, 1980). Why such crystal growth phenomena should apparently be confined to the crystallization of massif anorthosite is a fundamental and unanswered question. However, the restriction of OPMs to such plagioclase-rich (=aluminous) environments implies that local difficulties in pyroxene nucleation may be responsible, leading to significant supercooling with respect to pyroxene (i.e, overstepping of a plagioclase + pyroxene cotectic boundary; cf. Dymek and Gromet, 1984). We emphasize that OPMs are not quench crystals formed by an abrupt drop in temperature but that they grew metastably because of undercooling below their equilibrium crystallization temperature. In this regard, the lunar analogy breaks down because the interpretation advocated for lunar pyroxene phenocrysts involves rapid heat loss upon magma extrusion (Dowty et al., 1974). An important additional contrast with OPMs is that the lunar pyroxenes achieved their aluminous compositions because of rapid growth in magmas in which plagioclase nucleation was suppressed, i.e., pyroxene grew before plagioclase. OPMs,

TABLE 5.—*Continued*

Anal. no.	9	10	11	12	13	14	15	16	17
Sample	100.3	216	026	077	214	197	211	209	199
Host	OPM	OPM	OPM	OPM	CPM	CPM	CPM	CPM	CPM
SiO_2	55.81	54.83	55.05	57.17	57.65	59.05	55.62	57.94	56.96
Al_2O_3	27.87	28.81	28.57	27.72	26.81	26.14	28.68	26.96	26.96
FeO	0.19	0.70	0.20	0.47	0.13	0.22	0.13	0.08	0.21
CaO	9.35	10.27	9.81	8.74	8.40	7.50	10.38	8.21	8.63
Na_2O	5.91	5.33	5.63	6.26	6.62	6.94	5.49	6.54	6.32
K_2O	0.40	0.30	0.31	0.47	0.34	0.58	0.38	0.59	0.50
BaO	0.01	0.02	0.03	0.06	0.00	0.07	0.02	0.02	0.04
Total	99.54	100.26	99.60	100.89	99.95	100.50	100.70	100.34	99.62
				Formula proportions based on 8 O atoms					
Si	2.522	2.471	2.489	2.548	2.585	2.629	2.489	2.588	2.568
Al	1.484	1.530	1.522	1.456	1.417	1.372	1.513	1.419	1.432
Fe	0.007	0.026	0.008	0.018	0.005	0.008	0.005	0.003	0.008
Ca	0.453	0.496	0.475	0.417	0.403	0.358	0.498	0.393	0.417
Na	0.518	0.466	0.494	0.541	0.575	0.599	0.476	0.566	0.552
K	0.023	0.017	0.018	0.027	0.019	0.033	0.022	0.034	0.029
Ba	0.001	0.000	0.001	0.001	0.000	0.001	0.000	0.000	0.001
Total	5.008	5.006	5.007	5.008	5.004	5.000	5.003	5.003	5.007
Mol% An	45.6	50.6	48.1	42.3	40.4	36.1	50.0	39.6	41.7

on the other hand, grew together with or after plagioclase, but in a local environment that was nonetheless Al-rich.

Finally, an additional factor that could contribute to the peculiar nature of pyroxene megacrysts relates to their common association with hydrous phases, not only at Labrieville, but also at Saint Urbain (Dymek and Gromet, 1984) and at other andesine anorthosite massifs in the Grenville Province, such as Allard Lake (Hargraves, 1962, and personal communication), Château-Richer (Feininger, 1993), and Lac Chaudiere (see Fig. 2 in Owens et al., 1993). Specifically, biotite (and hornblende to a lesser extent) is found with every OPM occurrence in these anorthosites, not only as small flakes at megacryst margins, but also as thin plates within lamellae. Even in the apparently anhydrous Nain Complex, Veblen and Bish (1988) noted small amounts of amphibole and biotite in the OPM that they investigated. Thus, it is possible that local concentrations of volatile elements played some role in producing the coarse size of the megacrysts, perhaps by aiding diffusion of pyroxene constituents through the melt.

The alternative interpretation: Evidence for a remote crystallization site

X_{Mg}. Some previous studies at other localities have indicated that OPMs may be more magnesian than matrix orthopyroxene and thus may have formed earlier (Emslie, 1980; Jaffe and Schumacher, 1985). However, our results indicate that this is not always the case. In fact, bulk OPMs may be even more Fe-rich than matrix pyroxene. Therefore, if X_{Mg} is regarded as a reliable indicator of the timing of crystallization, then OPMs and matrix pyroxene appear to have formed at approximately the same time, from magmas of similar X_{Mg}. Furthermore, the occurrence of OPMs that are more Fe-rich than matrix orthopyroxene is consistent with the metastable growth of OPMs due to undercooling.

Al. The interpretation of pyroxene megacrysts as relics of high-pressure crystallization from basaltic magmas is based primarily on their aluminous bulk compositions, and we recognize that the influence of pressure on Al solubility in orthopyroxene was demonstrated long ago (Boyd and England, 1960). In further support of the high-pressure interpretation, Fram and Longhi (1992) and Longhi et al. (1993) documented experimentally a pressure-induced increase in Al_2O_3 in orthopyroxene in plagioclase-saturated melts. We cannot dispute these results, but we note that these experiments were conducted under anhydrous and reducing conditions (in graphite capsules). As such, these experiments are inappropriate for evaluation of OPM origins at Labrieville and Saint Urbain, where ubiquitous biotite and hematite-rich ilmenite indicate H_2O-bearing, oxidizing magmatic conditions (Anderson, 1966; Dymek and Schiffries, 1987). The oxidized nature of these massifs, in particular, may have some bearing on the properties of OPMs. Specifically, the ilmenite lamellae imply the presence of significant Fe^{3+} in the original pyroxene, which may have been incorporated as an $NaFe^{3+}Si_2O_6$ (acmite) or $MgFe^{3+}AlSiO_6$ component. With regard to the latter, the experiments of Arima (1978) demonstrated that (1) the solubility of Al in enstatite by the substitution $MgSi = Fe^{3+}Al$ increases with increasing temperature and decreasing pressure; and (2) at constant P and T, the solubility of Al_2O_3 increases with increasing Fe_2O_3. These results suggest that high temperatures and oxidizing conditions played a role in producing the compositions of megacrysts.

Compared with OPMs from anorthosites, orthopyroxenes in many high-pressure granulite terrains contain extreme amounts of Al_2O_3, locally up to 12 wt% (e.g., Bertrand et al., 1992), and yet never show plagioclase

exsolution despite slow decompression from depths of 10–12 kbar. In contrast, the bulk compositions of Labrieville and Saint Urbain OPMs are not unusually aluminous (4–6 wt% Al_2O_3). In addition, further work at Saint Urbain has shown that OPMs are not the most aluminous (nor the most magnesian) varieties in that massif. For example, pyroxenes in noritic rocks from the Saint Urbain ilmenite ore deposits are En_{75-80} with up to 9 wt% Al_2O_3, but they lack exsolution lamellae of plagioclase (Dymek, 1987). Collectively, these observations suggest that (1) high Al alone is insufficient to cause extensive exsolution of plagioclase in orthopyroxene; (2) the effect of decompression is probably minor relative to that of cooling from high temperature for the process of exsolution; and (3) high Al in orthopyroxene is not necessarily diagnostic of growth at high pressure.

Cr. In a few cases, OPMs have been shown to contain higher Cr than other orthopyroxene in a given anorthosite massif (Harp Lake, Labrador: 680–1570 ppm in OPMs, <600 ppm in interstitial orthopyroxene, Emslie, 1980; Egersund-Ogna, Norway: 600–950 ppm in OPMs, <600 ppm in orthopyroxene from medium-grained leuconorite, Duchesne et al., 1985). This observation was interpreted to indicate early (remote) crystallization of the OPMs from a magma more primitive than that which produced the other orthopyroxenes.

Labrieville OPMs (and CPM) contain relatively low Cr (≤350 ppm as determined by XRF, Table 4). These values are near or below the detection limit of the electron microprobe, and most analyses of matrix orthopyroxene at Labrieville show little or no detectable Cr (Table 2). At Saint Urbain, bulk OPMs contain 567–777 ppm Cr (Table 4). Although these levels are higher than at Labrieville, they correspond to Cr_2O_3 values of only 0.08–0.11 wt%, which are within the range found for other orthopyroxene in that massif by electron microprobe methods (Dymek and Gromet, 1984). Thus, as best we can determine, there is no clear enrichment of Cr in OPMs vs. matrix orthopyroxene at Labrieville or Saint Urbain.

Another significant factor concerning Cr distributions is the widespread association of ilmenite with OPMs at Labrieville and Saint Urbain. The Cr concentration in a bulk ilmenite sample from Labrieville is ~600 ppm (Owens, 1992), a factor of 2–6 higher than in the OPMs. Similarly, bulk ilmenite at Saint Urbain has Cr concentrations up to 1500 ppm (Dymek, unpublished data). On textural grounds, it appears that ilmenite crystallized along with OPMs in many cases. Thus, a depletion of Cr in matrix orthopyroxene compared with OPMs could simply reflect selective uptake of Cr into the iron titanium oxide phase.

The distribution of Cr in OPMs was explored recently by Longhi et al. (1993), using solute-rejection calculations based on the approach of Smith et al. (1955). Their results suggest that rapid growth should lead to an enrichment in Al (an incompatible element) in the growing pyroxene, concomitant with a depletion in Cr (a compatible element) relative to equilibrium values. These authors reasoned that if megacrysts grew rapidly, they should have higher Al but lower Cr compared with matrix pyroxene grown at equilibrium. The fact that OPMs in some massifs are enriched in both Al and Cr relative to matrix pyroxene was interpreted by Longhi et al. (1993) to be inconsistent with a rapid growth mechanism.

This approach to the evaluation of minor and trace element concentrations in OPMs is problematic on three accounts. First, the solute-rejection model of Smith et al. (1955) was developed originally to evaluate the distribution of impurities in simple metallurgical systems, wherein a metal crystallizes from a melt of its own composition. However, Shimizu (1981, 1983) demonstrated that minor-element distributions in zoned augite phenocrysts grown in silicate melt did not match the distributions predicted by the solute-rejection models. Shimizu (1981) accounted for this discrepancy by noting that the models assume an equilibrium condition at the surface of the growing crystal, with elemental partitioning dependent only on crystal growth rate and chemical diffusivity in the melt. Shimizu's results indicate, on the other hand, that kinetic processes at the crystal-melt interface can exert a significant control on elemental partitioning in rapidly grown crystals (see Nakamura, 1973; Shimizu, 1981, 1983; and Dymek and Gromet, 1984, for additional discussion). To these observations, we add that the solute-rejection models do not take charge-balance constraints into consideration and thus ignore a fundamental aspect of element partitioning into pyroxene (see below).

Second, even if the theoretical crystallization models apply, they are designed to predict compositional zoning patterns as a function of growth rate and provide little information about the absolute concentrations of elements in phenocrysts vs. matrix grains. As noted above, rapidly grown lunar pyroxenes contain higher Al and Cr (and Ti) relative to pyroxene grown under equilibrium conditions. Furthermore, groundmass pyroxene in the lunar samples is typically low in Cr, presumably in part because of previous Cr depletion in the magma by the growing pyroxene phenocrysts (and oxides; cf. Dalton and Hollister, 1974).

A final factor bearing on the incorporation of Cr into pyroxene is the precise substitutional mechanism involved. Substitution of Cr^{3+} for R^{2+} cations on the M1 site results in a charge excess that must be compensated for by a charge deficiency on tetrahedral sites involving the replacement of Si^{4+} by Al^{3+} (a Cr-Tschermak exchange, or $CrAlMg_{-1}Si_{-1}$). Thus, although Cr is typically considered compatible in pyroxene, this compatibility necessarily involves a coupled substitution with Al. In the OPMs, the main substituent is Al^{3+} on tetrahedral sites. Therefore, an enrichment of Cr in OPMs may represent but one example of scavenging by the crystal of any available R^{3+4+} cations in the melt needed to charge balance $^{[4]}Al$, in a fashion similar to that noted above for lunar pyroxenes. Thus, higher Cr in OPMs, where ob-

served, is not only consistent with but is the expected consequence of a rapid growth mechanism.

OPMs and host anorthosite as cotectic nodules: An unlikely compromise

Wiebe (1986) recognized that the subophitic textures of OPMs described by Morse (1975) and Dymek and Gromet (1984) indicated approximately simultaneous growth of plagioclase and pyroxene. To reconcile this observation with high-pressure crystallization of OPMs, Wiebe suggested that the megacrysts and surrounding plagioclase represent composite, high-pressure cotectic nodules transported intact to shallower levels. This interpretation is difficult to apply at Labrieville, however, in part because megacrystic pyroxene is so abundant (Fig. 1), which would imply that much of the massif consists of nodules. A more serious problem is the common association of pyroxene megacrysts with ilmenite. The intergrowths of these two minerals indicate simultaneous (or nearly so) crystallization, and it is unlikely that such dense masses could be rafted upward as xenolithic blocks.

At Saint Urbain, similar objections can be raised to the nodule hypothesis. Initially, OPMs were recognized in two domains—coarse-grained anorthosite and medium-grained subophitic leuconorite (Dymek and Gromet, 1984). This apparent areal restriction of OPMs could be construed as supporting the cotectic nodule interpretation. However, subsequent field work revealed the occurrence of several dozen additional OPM localities distributed throughout the massif. Many of these OPMs are found in pegmatoid patches up to ~1 m across, where lamella-bearing orthopyroxene megacrysts (10–30 cm across) occur with masses of coarse granular ilmenite, prominent books of biotite, minor quartz, and potassium feldspar. Such OPMs are clearly the products of late-stage, in-situ crystallization.

Implications of local crystallization for massif anorthosite petrogenesis

Current models for the origin of massif anorthosite invoke the pooling of basaltic magma in the deep crust or upper mantle, followed by fractionation of olivine and pyroxene, which remain at depth as an ultramafic cumulate, while plagioclase-rich mushes or feldspathic liquids rise to shallower levels to form anorthosite (e.g., Morse, 1982; Emslie, 1985; Ashwal, 1993). The fact that the ultramafic cumulates remain hidden at depth makes such models, regardless of their plausibility, difficult to test. Pyroxene megacrysts have thus achieved a certain prominence in anorthosite petrogenesis, for if they are indeed high-pressure crystals entrained during ascent, they could be fragments of the missing ultramafic cumulate.

In contrast, we regard the pyroxene megacrysts at Labrieville as the products of in-situ crystallization. Our field and petrographic observations indicate that OPMs grew after adjacent plagioclase in many cases, not before. Of course, the Labrieville parental magma may have experienced some fractionation history prior to final emplacement. However, the OPMs themselves provide no evidence for such a history, nor do they provide a link with a parental basaltic magma, in our opinion.

One of the most significant implications of our interpretation is that it requires cocrystallization at Labrieville of relatively magnesian OPMs, as well as associated matrix pyroxene (all $\sim En_{65}$), with highly alkalic plagioclase ($\sim An_{30}Or_{12}$: Owens, 1992). This An-En paradox, first recognized by Anderson and Morin (1969), characterizes numerous andesine anorthosites, as well as associated jotunites and mangerites in the Grenville Province, and serves as one major mineralogical distinction between this rock suite and differentiated basaltic intrusions (see Fig. 10 in Owens et al., 1993). Although the association of evolved plagioclase with magnesian pyroxene has been attributed to crustal contamination (e.g., Gray, 1987), the isotopic data presented in Owens et al. (1994) demonstrate that this is not the case at Labrieville. Hence, the An-En paradox must be a characteristic of the Labrieville parental magma—or at least it tells us something fundamental about the course of crystallization of that magma. By implication, we suggest that other andesine anorthosites having An-En relationships like Labrieville (e.g., Saint Urbain, Allard Lake, Château-Richer, Lac Chaudiere, etc.) may share a common petrogenesis.

In this regard, we consider the abundance of ilmenite at Labrieville (and other andesine anorthosites) to be an important clue, not necessarily to the composition of the parental magma, which remains elusive, but to the crystallization conditions of that magma. Specifically, the ubiquity of ilmenite, with its Fe_2O_3-rich composition ($\sim Ilm_{72}Hem_{28}$: Owens, 1992), suggests oxidizing magmatic conditions, as noted above. The relatively early separation of iron titanium oxide (perhaps as an immiscible oxide liquid; cf. Anderson, 1966) provides a convenient way to inhibit Fe enrichment in pyroxene. Thus, the relatively Mg-rich compositions of OPMs serve to highlight what we feel is the prominent role played by iron titanium oxide during the evolution of at least some massif anorthosites.

Acknowledgments

The research reported here was supported primarily by funds from Washington University. Additional support for laboratory work was provided by NSF grants EAR-8816977 and EAR-9019366 to R.F.D. Additional support for field work was provided by a Sigma Xi grant to B.E.O. We thank Rex Couture and Dan Kremser, Washington University, for the analytical support of the X-ray fluorescence and electron microprobe laboratories, respectively. L.D. Ashwal, J.H. Berg, R.F. Emslie, and B.L. Jolliff provided constructive reviews of earlier versions of this paper, and we thank Ron Emslie for bringing the study of Arima (1978) to our attention.

References cited

Anderson, A.T., Jr. (1966) Mineralogy of the Labrieville anorthosite, Quebec. American Mineralogist, 51, 1671–1711.

Anderson, A.T., Jr., and Morin, M. (1969) Two types of massif anorthosites and their implications regarding the thermal history of the crust. In Y.W. Isachsen, Ed., Origin of anorthosite and related rocks, p. 57–60. New York State Museum and Science Service, Memoir 18, Albany, New York.

Arima, M. (1978) Phase equilibria in the system $MgSiO_3$-Al_2O_3-Fe_2O_3 at high temperatures and pressures, with special reference to the solubility of Al_2O_3 and Fe_2O_3 in enstatite. Journal of the Faculty of Science, Hokkaido University, series IV, 18, 305–338.

Ashwal, L.D. (1993) Anorthosites, 422 p. Springer-Verlag, Berlin.

Bence, A.E., Papike, J.J., and Prewitt, C.T. (1970) Apollo 12 clinopyroxenes: Chemical trends. Earth and Planetary Science Letters, 8, 393–399.

Bence, A.E., Papike, J.J., and Lindsley, D.H. (1971) Crystallization history of clinopyroxenes in two porphyritic rocks from Oceanus Procellarum. Proceedings of the Second Lunar Science Conference, 1, 559–574.

Bertrand, P., Ouzegane, K., and Kienast, J.R. (1992) *P-T-X* relationships in the Precambrian Al-Mg-rich granulites from In Ouzzal, Hoggar, Algeria. Journal of Metamorphic Geology, 10, 17–31.

Bohlen, S.R., and Essene, E.J. (1978) Igneous pyroxenes from metamorphosed anorthosite massifs. Contributions to Mineralogy and Petrology, 65, 433–442.

Boyd, F.R., and England, J.L. (1960) Aluminous enstatite. Carnegie Institution of Washington Year Book, 59, 49–52.

Bryan, W.B., Finger, L.W., and Chayes, F. (1969) Estimating proportions in petrographic mixing equations by least-squares approximation. Science, 163, 926–927.

Champness, P.E., and Lorimer, G.W. (1976) Exsolution in silicates. In H.-R. Wenk, Ed., Electron microscopy in mineralogy, p. 174–204. Springer-Verlag, New York.

Couture, R.A., Smith, M.S., and Dymek, R.F. (1993). X-ray fluorescence analysis of silicate rocks using fused glass discs and a side-window Rh source tube: Accuracy, precision and reproducibility. Chemical Geology, 110, 315–328.

Dalton, J., and Hollister, L.S. (1974) Spinel-silicate co-crystallization relations in sample 15555. Proceedings of the Fifth Lunar Science Conference, 1, 421–429.

Dowty, E. (1980) Crystal growth and nucleation theory and the numerical simulation of igneous crystallization. In R.B. Hargraves, Ed., Physics of magmatic processes, p. 419–485. Princeton University Press, Princeton, New Jersey.

Dowty, E., Keil, K., and Prinz, M. (1974) Lunar pyroxene-phyric basalts: Crystallization under supercooled conditions. Journal of Petrology, 15, 419–453.

Duchesne, J.-C., Maquil, R, and Demaiffe, D. (1985) The Rogaland anorthosites: Facts and speculations. In A.C. Tobi and J.L.R. Touret, Eds., The deep proterozoic crust in the north Atlantic provinces, p. 449–476. Reidel, Boston.

Dymek, R.F. (1987) Petrogenetic implications of pyroxene compositional trends in the St. Urbain anorthosite complex and associated rocks, Quebec. Geological Society of America Abstracts with Programs, 19, 650.

Dymek, R.F., and Gromet, L.P. (1984) Nature and origin of orthopyroxene megacrysts from the St-Urbain anorthosite massif, Quebec. Canadian Mineralogist, 22, 297–326.

Dymek, R.F., and Schiffries, C.M. (1987) Calcic myrmekite: Possible evidence for the involvement of water during the evolution of andesine anorthosite from St-Urbain, Quebec. Canadian Mineralogist, 25, 291–319.

Emslie, R.F. (1975) Pyroxene megacrysts from anorthositic rocks: New clues to the sources and evolution of the parent magmas. Canadian Mineralogist, 13, 138–145.

——— (1980) Geology and petrology of the Harp Lake complex, central Labrador: An example of Elsonian magmatism. Geological Survey of Canada Bulletin, 293, 1–136.

——— (1985) Proterozoic anorthosite massifs. In A. Tobi and J.L.R. Touret, Eds., The deep proterozoic crust in the north Atlantic provinces, p. 39–60. Reidel, Boston.

Feininger, T. (1993) Geology and geophysics of the "type" anorthosite, Château-Richer, Quebec. Canadian Mineralogist, 31, 849–859.

Fram, M.S., and Longhi, J. (1992) Phase equilibria of dikes associated with Proterozoic anorthosite complexes. American Mineralogist, 77, 605–616.

Goodwin, A.M. (1992) Precambrian geology, 666 p. Academic, London.

Gray, C.M. (1987) Strontium isotopic constraints on the origin of Proterozoic anorthosites. Precambrian Research, 37, 173–189.

Grove, T.L., and Bence, A.E. (1977) Experimental study of pyroxene-liquid interaction in quartz-normative basalt 15597. Proceedings of the Eighth Lunar Science Conference, 2, 1549–1579.

——— (1979) Crystallization kinetics in a multiply saturated basalt magma: An experimental study of Luna 24 ferrobasalt. Proceedings of the Tenth Lunar Science Conference, 1, 439–478.

Grove, T.L, and Raudsepp, M. (1978) Effects of kinetics on the crystallization of quartz normative basalt 15597: An experimental study. Proceedings of the Ninth Lunar Science Conference, 1, 585–599.

Hargraves, R.B. (1962) Petrology of the Allard Lake anorthosite suite. In A.E.J. Engel et al., Eds., Petrologic studies (Geological Society of America Buddington Volume), p. 163–189, Boulder, Colorado.

Hollister, L.S., and Hargraves, R.B. (1970) Compositional zoning and its significance in pyroxenes from two coarse grained Apollo 11 samples. Proceedings of the Apollo 11 Lunar Science Conference, 1, 541–550.

Hollister, L.S., Trzcienski, W.E., Jr., Hargraves, R.B., and Kulick, C.G. (1971) Petrogenetic significance of pyroxenes in two Apollo 12 samples. Proceedings of the Second Lunar Science Conference, 1, 529–557.

Jaffe, H.W., and Schumacher, J.C. (1985) Garnet and piagioclase exsolved from aluminum-rich orthopyroxene in the Marcy anorthosite, northeastern Adirondacks, New York. Canadian Mineralogist, 23, 457–478.

Lofgren, G., Donaldson, C.H., Williams, R.J., Mullins, O., Jr., and Usselman, T.M. (1974) Experimentally reproduced textures and mineral chemistry of Apollo 15 quartz normative basalts. Proceedings of the Fifth Lunar Science Conference, 1, 549–567.

Longhi, J., Fram, M.S., Vander Auwera, J., and Montieth, J.N. (1993) Pressure effects, kinetics, and rheology of anorthositic and related magmas. American Mineralogist, 78, 1016–1030.

Maquil, R., and Duchesne, J.-C. (1984) Geothermométrie par les pyroxenes et mise en place du massif anorthositique d'Egersund-Ogna (Rogaland, Norvège Méridionale). Societè Géologique Belgique Annales, 107, 27–49.

Michot, P. (1939) La couronne d'anorthosite hypersthénifère feulletée et rubanée du massif anorthositique d'Egersund (Norvège). Societè Géologique Bilgique Annales, 62, 547–551.

Morse, S.A. (1975) Plagioclase lamellae in hypersthene, Tikkoatokhakh Bay, Labrador. Earth and Planetary Science Letters, 26, 331–336.

——— (1982) A partisan review of Proterozoic anorthosites. American Mineralogist, 67, 1087–1100.

Nakamura, Y. (1973) Origin of sector-zoning in igneous clinopyroxenes. American Mineralogist, 58, 986–990.

Owens, B.E. (1992) Petrogenesis of massif anorthosite: Mineralogical and geochemical constraints from the Labrieville massif, Quebec, 406 p. Ph.D. thesis, Washington University, Saint Louis, Missouri.

Owens, B.E., and Dymek, R.F. (1992) Fe-, Ti- and P-rich rocks and massif anorthosite: Problems of interpretation illustrated from the Labrieville and St-Urbain plutons, Quebec. Canadian Mineralogist, 30, 163–190.

Owens, B.E., Rockow, M.W., and Dymek, R.F. (1993) Jotunites from the Grenville Province, Quebec: Petrological characteristics and implications for massif anorthosite petrogenesis. Lithos, 30, 57–80.

Owens, B.E., Dymek, R.F., Tucker, R.D., Brannon, J.C., and Podosek, F.A. (1994) Age and radiogenic isotopic composition of a late- to post-tectonic anorthosite in the Grenville Province: The Labrieville massif, Quebec. Lithos, 31, 189–206.

Philpotts, A.R. (1966) Origin of anorthosite-mangerite rocks of southern Quebec. Journal of Petrology, 7, 1–64.

Rivers, T., Martignole, J., Gower, C.F., and Davidson, A. (1989) New tectonic divisions of the Grenville Province, southeast Canadian Shield. Tectonics, 8, 63–84.

Savolahti, A. (1966) The differentiation of gabbro-anorthosite intrusions and the formation of anorthosites. Comptes Rendus da la Societe geologique de Findlande, 38, 173–197.

Shimizu, N. (1981) Trace element incorporation into growing augite phenocryst. Nature, 289, 575–577.

——— (1983) Interface kinetics and trace element distribution between

phenocrysts and magma. In S.S. Augustithis, Ed., The significance of trace elements in solving petrogenetic problems and controversies, p. 175–195. Theophrastus, Athens, Greece.

Smith, V.G., Tiller, W.A., and Rutter, J.W. (1955) A mathematical analysis of solute redistribution during solidification. Canadian Journal of Physics, 33, 723–745.

Veblen, D.R., and Bish, D.L. (1988) TEM and X-ray study of orthopyroxene megacrysts: Microstructures and crystal chemistry. American Mineralogist, 73, 677–691.

Weill, D.F., Grieve, R.A., McCallum, I.S., and Bottinga, Y. (1971) Mineralogy-petrology of lunar samples: Microprobe studies of 12021 and 12022; viscosity of melts of selected lunar compositions. Proceedings of the Second Lunar Science Conference, 1, 413–430.

Wiebe, R.A. (1986) Lower crustal cumulate nodules in Proterozoic dikes of the Nain Complex: Evidence for the origin of Proterozoic anorthosites. Journal of Petrology, 27, 1253–1275.

Wynne-Edwards, H.R. (1972) The Grenville Province. In Variations in tectonic styles in Canada. Geological Association of Canada Special Paper, 11, 263–334.

Manuscript received May 3, 1994
Manuscript accepted September 15, 1994